HHS Public Access

Author manuscript

Phys Med Biol. Author manuscript; available in PMC 2017 August 07.

Published in final edited form as:

Phys Med Biol. 2016 August 7; 61(15): 5741–5754. doi:10.1088/0031-9155/61/15/5741.

Elasticity mapping of murine abdominal organs *in vivo* using Harmonic Motion Imaging (HMI)

Thomas Payen[1], **Carmine F. Palermo**[2], **Steve Sastra**[2], **Hong Chen**[1], **Yang Han**[1], **Kenneth P. Olive**[2,*], and **Elisa E. Konofagou**[1,3,*]

[1]Biomedical Engineering, Columbia University, USA

[2]Departments of Medicine and Pathology & Cell Biology, Herbert Irving Comprehensive Cancer Center, Columbia University Medical Center, USA

[3]Department of Radiology, Columbia University, USA

Abstract

Recently, ultrasonic imaging of soft tissue mechanics has been increasingly studied to image otherwise undetectable pathologies. However, many underlying mechanisms of tissue stiffening remain unknown, requiring small animal studies and adapted elasticity mapping techniques. Harmonic motion imaging (HMI) assesses tissue viscoelasticity by inducing localized oscillation from a periodic acoustic radiation force. The objective of this study was to evaluate the feasibility of HMI for *in vivo* elasticity mapping of abdominal organs in small animals. Pathological cases, i.e. chronic pancreatitis and pancreatic cancer, were also studied *in vivo* to assess the capability of HMI for detection of the change in mechanical properties. A 4.5-MHz focused ultrasound transducer (FUS) generated an amplitude-modulated beam resulting in 50-Hz harmonic tissue oscillations at its focus. Axial tissue displacement was estimated using 1D-cross-correlation of RF signals acquired with a 7.8-MHz diagnostic transducer confocally aligned with the FUS. In vitro results in canine liver and kidney showed the correlation between HMI displacement and Young's moduli measured by rheometry compression tests. HMI was able to provide reproducible elasticity maps of the mouse abdominal region *in vivo* allowing the identification of, from stiffest to softest, the murine kidney, pancreas, liver, and spleen. Finally, pancreata affected by pancreatitis and pancreatic cancer showed HMI displacements 1.7 and 2.2 times lower than in the control case, respectively, indicating higher stiffness. HMI displacement was correlated with the extent of fibrosis as well as detecting the very onset of stiffening even before fibrosis could be detected on H&E. This work shows that HMI can produce reliable elasticity maps of mouse abdominal region *in vivo* providing a crucial tool to understand pathologies affecting organ elasticity.

Introduction

Palpation has been a standard medical practice for qualitative assessment of tissue stiffness since the earliest recorded days of medicine. Many otherwise undetectable abdominal pathologies result in tissue stiffness changes, and in certain cases, stiffness correlates with disease severity. For example, many cancers can be detected as stiff masses surrounded by

*Co last authors

softer normal tissue. However, detection and evaluation by palpation can be difficult or impossible due to lesion size, stiffness, and/or location. In addition, diffuse diseases such as pancreatitis may increase the stiffness of the whole organ without distinctive contrast.

Tissue mechanical properties can be assessed with non-destructive and non-invasive, quantitative elastography *in situ*. These techniques generate a mechanical perturbation in the targeted tissue and infer its mechanical properties from its monitored response. The perturbation can be externally-generated as in quasi-static (Ophir et al. 2002), transient (Sandrin et al. 2003) and dynamic elastography (Parker et al. 1990; Shi et al. 1999) or Magnetic Resonance Elastography (MRE) (Godfrey et al. 2013; Kruse et al. 2000; Muthupillai et al. 1995). Other techniques use internal stimulus as in vibroacoustography (Fatemi and Greenleaf 1998), Shear Wave Elastography (SWE) (Barry et al. 2012; Barry et al. 2014; Bercoff et al. 2004; Chen et al. 2013; Sapin-de Brosses et al. 2011; Sarvazyan et al. 1998; Zhu et al. 2014) and Acoustic Radiation Force Impulse (ARFI) imaging (Nightingale et al. 2001). Several studies have shown the clinical feasibility of elasticity imaging to assess mechanical properties of different soft tissues such as the breast (Bercoff et al. 2003), the arterial wall (Couade et al. 2010) and the liver (Wang et al. 2012).

However, many underlying mechanisms of tissue stiffening remain unknown. Animal models, and in particular rodents, are necessary in this context to understand the implications of mechanical properties on the state of the studied tissue. These small animal studies require high spatial resolution due to the small volume of the targets and high temporal resolution due to faster physiological functions. To our knowledge, few studies have addressed the assessment of mechanical properties in abdominal organs of small animals for these reasons, and even fewer, if any, have been able to provide a map showing their elasticity.

Elastography has been used in small animals *in vivo* mostly for liver stiffness estimation with transient micro-elastography (TME) (Bastard et al. 2011), MRE (Salameh et al. 2009; Yin et al. 2007b), ARFI (Wang et al. 2009), and SWE (Chia-Lun Yeh et al. 2014). These studies estimate the extent of liver stiffening due to fibrosis and/or steatosis with good agreement compared to the reference histology analysis. *In vitro* studies also showed the potential of elastography for viscoelastic assessment of small animal fibrotic liver using shear wave dispersion as a function of frequency (Barry et al. 2012; Barry et al. 2014; Chen et al. 2013; Zhu et al. 2014). Kidney stiffness was assessed in rats using MRE in the case of nephrocalcinosis (Shah et al. 2004) and with SWE for glomerulosclerosis (Derieppe et al. 2012). Both studies report stiffening according to the pathology progression. However, to the best of our knowledge, there is no study in small animals regarding elastography applied to the spleen and the pancreas, nor comparing different abdominal organs. Moreover, out of all the aforementioned articles, only two show elasticity-based maps (Salameh et al. 2009; Yin et al. 2007b), both in the largest organ, i.e. the liver, with a resolution too low to distinguish different tissues. This void is due to the characteristics of these techniques limiting their use in small animals. TME requires a relatively large, superficial, and homogeneous tissue, which limited its use for point-by-point assessment of the liver. MRE remains very expensive, preventing its routine use in animal laboratories. The small scale also limits the

use of propagation-based techniques such as SWE. The geometry of abdominal organs also makes the shear wave signal very complex.

Harmonic Motion Imaging (HMI) assesses tissue viscoelasticity by inducing localized oscillation resulting from an amplitude-modulated acoustic radiation force (Konofagou and Hynynen 2003; Maleke et al. 2006). An imaging probe is confocally aligned with the focused ultrasound transducer (FUS). Frame-to-frame displacement is assessed using a 1D cross-correlation algorithm. The amplitude of the displacement is directly related to the underlying tissue stiffness. HMI has several advantages. First, the imaging component of the system may be any commercially-available clinical imaging probe. Second, the FUS transducer uses high power output which can assess deep organs and a wide range of stiffness. In addition, noise, speed of sound variation and physiologic motion can easily be filtered out due to the specific AM frequency of the displacement signal. In the context of small animal studies with small targets, HMI benefits from probing directly at the focal region at a submillimetric scale. An additional advantage of HMI over ARFI is that it can provide real-time feedback during the force application at the transducer focus, which is of particular interest when coupled to High-Intensity Focused Ultrasound (HIFU) treatment for monitoring without interruption of the high-intensity beam and adaptively adjusting the dose delivered.

HMI has recently been shown capable of assessing the elastic properties of biological tissues, and its feasibility has been demonstrated in polyacrylamide gels and in *ex vivo* canine liver specimens (Vappou et al. 2015). The stiffness index introduced in this study, E_{HMI}, was very well correlated to the Young's modulus in numerical simulation ($r^2 > 0.99$) and tissue mimicking phantoms ($r^2 = 0.95$). Although Young's modulus is not directly quantified, this study showed that HMI displacement can serve as a qualitative marker reflecting the elasticity of different types of tissue. Another study from Chen et al. (Chen et al. 2015a) showed the *in vivo* feasibility of HMI assessment without damage to the tissue using a 2.5-MHz imaging probe in the case of a murine model for pancreatic tumor. The normal pancreas showed HMI displacement 3.2 times higher than the malignant pancreas.

This study investigates the feasibility of HMI as an *in vivo* elasticity mapping technique for abdominal organs in mice. For this purpose, a 7.8-MHz imaging probe was implemented in order to be able to acquire higher resolution elasticity maps. The first objective of this paper was to validate HMI displacement values against Young's modulus measured with rheometry *in vitro* in canine organs. The second part focused on evaluating the *in vivo* feasibility of HMI for elasticity mapping of mouse abdominal organs. Finally, the third objective was to use HMI to discriminate healthy from pathological organs in the case of chronic pancreatitis and pancreatic ductal carcinoma (PDA).

Material and methods

1. HMI setup

The system is briefly described in this article (Figure 1). For more details, please refer to our group's previous publications (Hou et al. 2014). A 93-element phased array transducer (H-178, Sonic Concept Inc. Bothell WA, USA) was used in this study to generate the

acoustic force at the focus. The −6 dB focal region has an ellipsoid shape with 1.35 mm in the axial direction and 0.25 mm in the lateral direction. A dual-channel arbitrary waveform generator (AT33522A, Agilent Technologies Inc., Santa Clara, CA, USA) sent an amplitude-modulated (AM) signal ($f_{carrier}$ = 4.5 MHz and f_{AM} = 25 Hz) to drive all 93 channels simultaneously after amplification by a nominal 50-dB gain power amplifier (325LA, E&I, Rochester, NY, USA). The resulting beam generated a 50-Hz harmonic tissue oscillatory motion at the transducer focus. The FUS acoustic power measured in water was 5.04 W.

Axial tissue displacement was estimated using RF signals acquired with a 104-element diagnostic transducer (P12-5, ATL/Philips, Bothell, WA, USA, fc = 7.8 MHz) confocally aligned with the FUS transducer. A Vantage 256 system (Verasonics, Bothell, WA, USA) was used to operate the imaging probe in a plane-wave beam sequence with a framerate of 1 kHz.

A respiration gating system (Biopac System, Santa Barbara, CA, USA) was used to acquire data only in-between two breath-holds. Respiration was monitored using a pressure sensor linked to a MP150 Data Acquisition System. The analog signal from the MP150 was then converted to trigger the Vantage system, itself triggering the waveform generator for simultaneous sonication and data acquisition.

For each position, the FUS exposure lasted 0.2 s, during which 200 RF frames (10 oscillation cycles) were acquired. A GPU-based beamforming (Hou et al. 2014) was performed along with an upsampling to reach a 125 MHz sampling frequency. The FUS signal and its harmonic were then filtered out using two notch filters at 4.5 and 9 MHz. The axial displacement was estimated using a 1D cross-correlation algorithm (Luo and Konofagou 2010) along each lateral beam lines on consecutive frames. The correlation window was 0.98-mm long with 95% overlap. A bandpass filter around 50 Hz was applied to further reduce electronic noise. The median peak-to-peak displacement amplitude was calculated for each pixel.

For each tissue, 2 to 6 HMI measurements at different locations were probed. For each measurement, a ROI was manually drawn on the Bmode reconstructed from the RF data. The HMI values presented in this work are mean values ± standard deviation calculated on all the pixels selected in all measurements for each tissue. A two-tailed t-test with a threshold p-value of 0.05 was used to determine the significance of the difference in mean displacement.

2. Rheometry

Canine livers and kidneys were harvested on two freshly sacrificed control dogs used in other experiments. These organs were kept frozen 3 to 7 days before HMI assessment when they were thawed overnight and degassed in PBS before being pinned down to an absorber in a PBS tank. For each tissue, HMI measurements were performed in 6 locations separated by 3 mm.

A 6-mm biopsy punch was used to extract a total of 13 cylindrical samples right after the HMI scan (diameter = 4.90 ± 0.39 mm and height = 5.27 ± 1.33 mm) from the liver (n = 7),

and from the kidney (n = 3 from the external cortex region and n = 3 from the internal pelvis region). Mechanical testing was performed on these samples using compression rheometry (ARES-G2, TA Instrument, New Castle, DE, USA) in a static force gap test. The sample was placed in PBS between two stationary plates. A preliminary 10% compressional strain was applied to insure contact at the interfaces. Then, the stress was measured as the strain was increased by reducing the gap between the two plates. The Young's modulus was then calculated for each sample and plotted against its HMI displacement.

3. *In vivo* mouse protocol

In accordance with the National Institutes of Health Guidelines for animal research, all animal procedures were reviewed and approved by the Institutional Animal Care and Use Committee of the Columbia University. A total of 34 mice (age 8–20 weeks) were utilized in this study. Ten BalbC mice were used for the *in vivo* elasticity mapping, and 24 genetically engineered mice were used for the pathological study in which the control results were provided with the previously mentioned 10 BalbC mice.

All the animals were anesthetized with 1–2% isoflurane in oxygen throughout the whole procedure, which lasted less than 1 hour. The mice were placed in supine position on a heating pad with their abdomen depilated. A container filled with degassed water was placed with an acoustically-transparent window above their abdomen and coupled with degassed ultrasound gel. For each animal, 2 to 4 planes separated by 1 mm in the elevation direction of the imaging probe were scanned depending on the size of the acoustic window available.

A 18.5-MHz diagnostic probe (L22-14v, Verasonics) was used to locate, and identify the different organs. A marker was then placed in the water container above the mouse for spatial correlation between the high-frequency images and the HMI system Bmode.

The HMI system was mechanically moved using a 3D positioner (Velmex Inc., Bloomfield, NY, USA) to probe each entire Bmode plane. Experiments in a homogeneous tissue-mimicking phantom (data not shown) have shown that the region engaged in oscillation (calculated as demonstrating 90% of the maximum displacement or more) was approximately $3.6 \times 4\ mm^2$. Thus, the raster scan was performed with 1.8 mm-lateral step and 2.0 mm-axial step for a total acquisition time of 30 seconds to cover a $12.6 \times 10\ mm^2$ imaging plane.

To reconstruct the entire imaging plane, the displacement amplitude maps from all positions were averaged with a weight attributed to each pixel according to its distance to the focal. In addition, attenuation was compensated by

$$D_z = D_{z_0} e^{2f\alpha(z_0 - z)}$$

where D_z and D_{z_0} are the displacements measured at depth z and at the focal depth z_0, f is the imaging frequency, and α is the attenuation coefficient fixed at 0.5 dB/cm/MHz (Chen et al. 2015b).

4. Chronic pancreatitis and PDA

K-ras$^{LSL.G12D/+}$; PdxCre$^{tg/+}$ mice (N = 14), also called KC mice, were used in this study (Hingorani et al. 2003). The KC mice are prone to developing pancreatic cancer ductal adenocarcinoma (PDA) at advanced ages (> 1yr). Prior to tumor onset, the pancreata of KC mice are prone to spontaneous inflammation (pancreatitis), and this can be dramatically exacerbated through administration of cerulein, a peptide analog of cholecystokinin. We treated 8 – 20 week old, tumor-free KC mice with cerulein (250mg/kg, i.p, daily for 5 days) to induce chronic pancreatitis (Ardito et al. 2012). One week after induction, the mice were handled and scanned as described in the previous section.

Following HMI, mice were euthanized and necropsied. The pancreas was prepared for H&E staining with care taken to maintain the head-tail orientation of the organ. Whole pancreas slides were examined under the microscope by a blinded expert with magnifications from ×4 to ×10. Fibrosis extent was calculated as a percentage area relative to the whole pancreatic surface. The mice were classified according to the % fibrotic area in 3 groups: 0–25%, 25–50% and over 50%.

In addition, five cases of PDA in a transgenic mouse model were also scanned. K-ras$^{LSL.G12D/+}$; p53$^{LSL.R172H/+}$; PdxCre$^{tg/+}$ (KPC) mice spontaneously develop PDA with a mean latency of 5.5 months (Hingorani et al. 2005). KPC mice develop tumors with pathophysiological and molecular characteristics similar to those present in human PDA. We identified tumor-bearing KPC mice through weekly palpation and high resolution ultrasound imaging, as previously described (Olive et al. 2009; Sastra and Olive 2013). Mice with tumors 3– 5 mm in diameter were used as described in the previous section.

Results

The results showed that HMI was capable of providing reproducible elasticity maps of the abdominal region *in vivo*. The technique was also able to differentiate pancreatitis from normal pancreas.

1. *In vitro*: HMI vs rheometry

The canine organ study showed excellent agreement ($R^2 > 0.99$) between mechanical testing and the HMI measurements (Figure 2). The Young's moduli of the liver, renal cortex and renal pelvis were 4.9 ± 1.4 kPa, 7.9 ± 1.3 kPa, and 13.1 ± 4.0 kPa, respectively, from the softest to the stiffest. The HMI results of these tissues were significantly different ($p < 0.05$) with mean displacements of 13.3 ± 0.5 μm, 11.1 ± 0.9 μm, and 8.1 ± 1.5 μm, respectively, properly reflecting the stiffness order observed with rheometry.

2. *In vivo* HMI mapping

HMI enabled the acquisition of *in vivo* elasticity maps in the mouse allowing abdominal organ identification, and the assessment of their elasticity. The results obtained in the spleen, the liver, the pancreas, and the kidney (from softest to stiffest) of 10 control mice are shown in Table 1. Significant difference ($p < 0.05$) was observed between the kidney and all the

other organs. The spleen was shown to be the softest organ, but results also showed high standard deviation. The pancreas and the liver demonstrated intermediate HMI values.

Figure 3 shows two imaging planes displaying different organs of the same mouse (called Mouse A). Plane #1 shows the kidney and the liver with intestines in between. The mean HMI displacements were significantly different for these two organs (8.3 ± 1.9 μm and 15.6 ± 2.2 μm, respectively, $p < 0.05$). These results confirm the rheometry measurements demonstrating that the liver is softer than the kidney. Imaging plane #2 displays the kidney, the pancreas and the spleen with significantly different HMI displacements (6.1 ± 1.2 μm, 11.6 ± 1.8 μm, and 18.8 ± 5.5 μm, respectively, $p < 0.05$). Values for intestines are not presented as delineation, and gaseous content hindered the calculation of reliable HMI displacement which was reflected by a low mean correlation coefficient (< 0.8).

The liver and the left kidney of Mouse A were then scanned *ex vivo* (Figure 4). The HMI displacements were measured at 14.2 ± 3.1 μm and 4.2 ± 1.0 μm, respectively ($p < 0.05$). This experiment confirms the range of values observed *in vivo* and the relative stiffness between these two organs.

3. Chronic pancreatitis and PDA

Overall, pancreata from transgenic mice injected with cerulein presented HMI displacements on the average 1.7 times lower than in the normal pancreas (7.3 ± 2.1 μm and 12.5 ± 2.6 μm, respectively, $p < 0.01$) indicating higher overall stiffness.

H&E staining allowed the quantification of fibrotic tissue across the entire pancreas as shown in Figure 5. About 85% of normal pancreatic tissue is composed of acinar cells (Hruban et al. 2007) which appear on H&E sections with an eosinophilic cytoplasm and an organized, regular pattern. By contrast, fibrotic pancreas tissue loses acinar cells through a process of acinar-to-ductal metaplasis, resulting in a disorganized appearance that lacks the intense pink stain of normal acinar cells. These two states are easily distinguished from low magnification, facilitating simple quantification of percent fibrotic pancreatic tissue.

When subdivided based on the extent of fibrosis (Figure 6), HMI was able to distinguish control from any extent of fibrosis. Even when the pancreas only presented low extent of fibrosis (< 25%), HMI picked up a significantly lower displacement (7.8 ± 2.4 μm, $p < 0.01$). HMI was sensitive enough to detect the early onset of stiffening even before fibrotic tissue appear (0% score in H&E staining). Moreover, HMI displacements were significantly lower for the severely fibrotic cases (> 50% fibrotic tissue) than the less severe cases (5.6 ± 0.7 μm versus 8.1 ± 2.0 μm, $p < 0.01$) indicating that decreased displacement correlates with severity of fibrosis in mice with pancreatitis.

Finally, the PDA cases demonstrated HMI displacements 2.2 times lower than in the control mice (5.6 ± 0.9 μm, $p < 0.001$). The PDA results were similar to those from the highly fibrotic group, and significantly lower than the below 50% fibrotic pancreata ($p < 0.01$).

Discussion

Elasticity assessment can provide critical information in the diagnosis of abdominal pathologies. However many underlying mechanisms of tissue stiffening remain unknown and require small animal studies. Elastography is not commonly used *in vivo* for abdominal mapping in small animals due to spatial resolution requirements, motion, heterogeneity, and boundary issues. This study demonstrates for the first time that HMI can provide reliable elasticity maps in mice reflecting the stiffness of abdominal organs in healthy animals as well as in pathological cases such as chronic pancreatitis and pancreatic cancer. This work shows that HMI can answer the need for an elastography technique for screening and small animal studies due to its low cost, efficient noise filtering and deep penetration. Moreover, previous work showed that the short duration of the acoustic exposure (0.2 s) prevents any damage to the tissue (Chen et al. 2015a).

The first part of this study validated the inverse relationship between HMI displacements and Young's modulus. Samples for rheometry were extracted from canine liver and kidney. The kidney was separated into two regions: the outer, softer cortex and the inner, stiffer pelvis. Rheometry showed that the liver is softer than the renal cortex, itself being softer than the renal pelvis in agreement with existing literature (Umale et al. 2012). HMI showed a similar relative stiffness between these three types of tissue with significantly different values of displacement. The ratio of the moduli was not accurately reflected in HMI, which is not surprising considering the fundamental differences between the two measurements especially the tissue sampling (biopsy punch versus whole organ), and the nature of the test (static versus dynamic). Moreover, non-linear effects may also explain this discrepancy. In many tissue, Young's modulus is dependent on the level of strain applied for measurement which is low for HMI and high for rheometry. In addition, perfusion should be maintained to reproduce the *in vivo* viscoelastic properties in *ex vivo* tissue. Lack of perfusion was shown to result in tissue stiffening (Kerdok et al. 2006).

This study then showed the feasibility of using HMI to acquire *in vivo* elasticity maps in the abdominal region of mice enabling to differentiate the organs based on their mechanical properties. In this work, the spleen, the liver, the pancreas, and the kidney were all probed and mapped based on their HMI displacement. The mean HMI displacements for these 4 organs *in vivo* were 18.3 ± 7.0 μm, 14.2 ± 2.1 μm, 12.3 ± 2.5 μm, and 6.3 ± 1.9 μm, respectively. The values for the kidney and the liver were validated *ex vivo*. Small animal studies measuring stiffness in different abdominal organs are lacking. Literature does exist in big animals and patients, but comparison with our results is limited because of the differences in organ structure (Dolenšek et al. 2015; Steiniger 2015). Moreover, definite conclusions on healthy abdominal organs relative stiffness remains to be determined. Across the literature and the different elastography techniques, the liver is commonly found to be relatively soft with a Young's modulus between 5 and 10 kPa (Bensamoun et al. 2011; Castera et al. 2010; Guo et al. 2014; Masuzaki et al. 2007; Palmeri et al. 2008; Yin et al. 2007a), when the kidney is admitted to be stiffer (Arda et al. 2011; Bensamoun et al. 2011; Gallotti et al. 2010; Gennisson et al. 2012) as observed in this study. However the stiffness of the spleen and the pancreas are not as well established. Using SWE in healthy volunteers, Arda et al. (Arda et al. 2011) showed that the spleen was softer (2.9 ± 1.8 kPa) than the

pancreas (4.8 ± 3 kPa), when Leung et al. (Leung et al. 2013) found the spleen to be much stiffer (17.3 ± 2.6 kPa) than the liver (5.5 ± 0.7 kPa). Results from different ARFI studies also measured a higher stiffness in the spleen than in the liver (Cabassa et al. 2015; Guo et al. 2014), the pancreas and even the kidney (Gallotti et al. 2010). More studies are needed to draw conclusions on the relative stiffness of abdominal organs both in human and small animal. In addition, studies have shown that intra-parenchymal pressure may impact tissue elasticity. Vizzutti et al. (Vizzutti et al. 2007) demonstrated the positive correlation between hepatic venous pressure gradient and liver stiffness in 61 patients with transient elastography. Gennisson et al. (Gennisson et al. 2012) showed that *in vivo* kidney elasticity increases with elevation of blood and urinary pressures using SWE in a pig model. The intra-parenchymal pressure should then be taken into account for complete interpretation of tissue changes *in vivo*.

A pathological case of chronic pancreatitis was also studied with HMI. Chronic pancreatitis is a progressive inflammatory disease of the pancreas, characterized by irreversible morphologic changes and gradual fibrotic replacement of the gland which induces stiffening. It is considered as one of the risk factors of pancreatic cancer (Lowenfels and Maisonneuve 2006), the fourth leading cause of cancer death with the worst prognosis of any major tumor type (Siegel et al. 2014). In our mouse model, inflamed pancreata demonstrated HMI displacements 1.7 times lower than normal pancreata (12.5 ± 2.6 μm vs 7.3 ± 2.1 μm). HMI was also able to differentiate low fibrosis extent from highly fibrotic pancreas (8.1 ± 2.0 μm vs 5.6 ± 0.7 μm with a 50% threshold). HMI detected the early onset of stiffening even prior to fibrotic appearance in histology. Further analysis with specific staining would be necessary to see if stiffening detection at earlier disease stages such as steatosis had already taken place in those organs. However, the early detection of pancreatitis using a technique fitted for screening such as HMI represents a major step in dealing with pancreatic cancer.

PDA cases displayed HMI displacements 2.2 times lower than the normal pancreata. These measurements were also significantly lower than the ones obtained in low fibrotic groups. Previous reports by our group (Chen et al. 2015a) also reported that the feasibility of this technique for *in vivo* tumor detection in the same PDA murine model with similar results. Normal pancreas showed HMI displacement 3.2 times higher than malignant pancreas. The small difference in ratio can be explained by the difference of systems, and the more advanced stage of the tumor (diameter > 5mm) used in previous reports.

HMI for abdominal elasticity mapping has a few limitations. First, an acoustic window and penetration are required. That is an issue for human abdominal organs as they may lie at a profound depth, with difficult acoustic access. Going through air-filled intestines affects the HMI measurement. The main consequence would be a loss of power and force at the focus together with potential defocusing. In this study, the acoustic path was always chosen on Bmode images in order to avoid air in the intestines. The HMI system is rather flexible in terms of positioning, and optimal acoustic windows can be found. This study demonstrated the capability of HMI to provide elasticity maps in different organs within the abdominal cavity. Another issue lies with the heterogeneity of the HMI displacements measured in some organs, in particular the shallow ones like the spleen. Smaller FUS focal coupled with higher imaging resolution would help reduce this variability. Boundary conditions as well as

attachment to surrounding organs may also affect the measurements as they impact the oscillation of the tissues probed. The shear wave component resulting from reflection was ignored in this study. This assumption is based on the small size of our focal (0.25 × 1.35 mm2) compared to the mouse organs, and the fact that our measurement are confined to the focal region. Attenuation and viscosity rapidly decrease the amplitude of the primary shear wave as it propagates outwards from the very small focal region. Our group has published on shear waves during HMI (Vappou et al. 2009) and shear waves are severely dampened from the HMI focus leading to negligible effects on the displacements measured. Only a small reflected component will make it back to the region of measurement. Quantifying the reflected shear wave contribution is a particularly complex issue as you need to know the exact geometry of the tissue as well as the characteristics of the boundaries. Finally, the organs are much smaller than the shear wavelength so resonance is not an issue. Another limitation is that the HMI displacement is dependent on the force applied, which is affected by the amplitude of the signal, the AM frequency, and the attenuation. In this study, we assumed a homogeneous, constant attenuation with $\alpha = 0.5$ dB/cm/MHz. Previous work from our lab (Vappou et al. 2015) have estimated the applied force by modeling the focal region as a cylindrical region inside which the volumetric acoustic radiation force is uniform. Future work will aim at refining this model in terms of force distribution and local tissue absorption to get closer to the real force profile and provide robust, quantitative viscoelastic moduli. Other methods such as Monitored Steady-State Excitation and Recovery (MSSR) aim to provide quantitative estimates of viscoelastic parameters independently of the force applied (Mauldin et al. 2008).

Further efforts will aim at implementing electronic beam steering to replace mechanical scanning which would help for the translation toward clinical screening purposes as the system could be maintained in one position and the scanning time would be decreased. Motion compensation can also be improved on. The main limit of the respiratory gating used in this work is that it does not correct for other motion sources such as heart beats and physiologic motion. A solution developed in MR-guided HIFU treatment is to use electronic beam steering for 3D motion compensation to remain within the targeted site whatever the motion is (Ries et al. 2010; Zachiu et al. 2015). This would require capability of tracking the target in real-time and in 3D, as well as adapting the focal position at a high temporal and spatial resolution with a low tracking latency to limit errors.

Conclusion

This study demonstrates that HMI can provide reliable elasticity maps *in vivo* accurately representing the relative stiffness of abdominal organs in healthy animals as well as in pathological cases such as chronic pancreatitis and pancreatic cancer. Based on acoustic force oscillations tracking, HMI was able to differentiate and localize the kidney, the pancreas, the liver, and the spleen *in vivo*. Moreover, HMI was applied to chronic pancreatitis and pancreatic cancer. HMI was capable of differentiating normal from inflammatory pancreata and pancreatic tumors, as well as staging the extent of fibrosis. More importantly, HMI was capable of detecting the early onset of stiffening even when fibrosis remained undetected in histology. The validation of HMI for elasticity mapping in

small animals represents an important step towards future clinical applications of HMI as a promising imaging technique with screening potential.

References

Arda K, Ciledag N, Aktas E, Aribas BK, Köse K. Quantitative assessment of normal soft-tissue elasticity using shear-wave ultrasound elastography. Am J Roentgenol. 2011; 197:532–536. [PubMed: 21862792]

Ardito CM, Grüner BM, Takeuchi KK, Lubeseder-Martellato C, Teichmann N, Mazur PK, DelGiorno KE, Carpenter ES, Halbrook CJ, Hall JC, Pal D, Briel T, Herner A, Trajkovic-Arsic M, Sipos B, Liou GY, Storz P, Murray NR, Threadgill DW, Sibilia M, Washington MK, Wilson CL, Schmid RM, Raines EW, Crawford HC, Siveke JT. EGF Receptor Is Required for KRAS-Induced Pancreatic Tumorigenesis. Cancer Cell. 2012; 22:304–317. [PubMed: 22975374]

Barry CT, Hah Z, Partin A, Mooney RA, Chuang KH, Augustine A, Almudevar A, Cao W, Rubens DJ, Parker KJ. Mouse liver dispersion for the diagnosis of early-stage fatty liver disease: A 70-sample study. Ultrasound Med Biol. 2014; 40:704–713. [PubMed: 24412179]

Barry CT, Mills B, Hah Z, Mooney RA, Ryan CK, Rubens DJ, Parker KJ. Shear wave dispersion measures liver steatosis. Ultrasound Med Biol. 2012; 38:175–182. [PubMed: 22178165]

Bastard C, Bosisio MR, Chabert M, Kalopissis AD, Mahrouf-Yorgov M, Gilgenkrantz H, Mueller S, Sandrin L. Transient micro-elastography: A novel non-invasive approach to measure liver stiffness in mice. World J Gastroenterol. 2011; 17:968–975. [PubMed: 21448348]

Bensamoun SF, Robert L, Leclerc GE, Debernard L, Charleux F. Stiffness imaging of the kidney and adjacent abdominal tissues measured simultaneously using magnetic resonance elastography. Clin Imaging Elsevier Inc. 2011; 35:284–287.

Bercoff J, Chaffai S, Tanter M, Sandrin L, Catheline S, Fink M, Gennisson JL, Meunier M. In vivo breast tumor detection using transient elastography. Ultrasound Med Biol. 2003; 29:1387–1396. [PubMed: 14597335]

Bercoff J, Tanter M, Fink M. Supersonic shear imaging: a new technique for soft tissue elasticity mapping. IEEE Trans Ultrason Ferroelectr Freq Control. 2004; 51:396–409. [PubMed: 15139541]

Cabassa P, Ravanelli M, Rossini A, Contessi G, Almajdalawi R, Maroldi R. Acoustic radiation force impulse quantification of spleen elasticity for assessing liver fibrosis. Abdom Imaging. 2015; 40:738–744. [PubMed: 25425490]

Castera L, Sebastiani G, Le Bail B, de Ledinghen V, Couzigou P, Alberti A. Prospective comparison of two algorithms combining non-invasive methods for staging liver fibrosis in chronic hepatitis C. J Hepatol European Association for the Study of the Liver. 2010; 52:191–198.

Chen H, Han Y, Payen T, Palermo C, Olive K, Konofagou E. Harmonic motion imaging in abdominal tumor detection and HIFU ablation monitoring: A feasibility study in a transgenic mouse model of pancreatic cancer. IEEE Trans Ultrason Ferroelectr Freq Control. 2015a; 62:923–926.

Chen J, Hou GY, Marquet F, Han Y, Camarena F, Konofagou E. Radiation-force-based estimation of acoustic attenuation using harmonic motion imaging (HMI) in phantoms and *in vitro* livers before and after HIFU ablation. Phys Med Biol IOP Publishing. 2015b; 60:7499–7512.

Chen X, Shen Y, Zheng Y, Lin H, Guo Y, Zhu Y, Zhang X, Wang T, Chen S. Quantification of liver viscoelasticity with acoustic radiation force: A study of hepatic fibrosis in a rat model. Ultrasound Med Biol. 2013; 39:2091–2102. [PubMed: 23993170]

Chia-Lun, Yeh; Bo-Rong, Chen; Ling-Yi, Tseng; Ping, Jao; Tung-Hung, Su; Li, P. Shear wave elastography of a liver fibrosis mouse model using a high frequency ultrasound system with mechanical scanning; 2014 IEEE Int Ultrason Symp; 2014. p. 1140-1143.

Couade M, Pernot M, Prada C, Messas E, Emmerich J, Bruneval P, Criton A, Fink M, Tanter M. Quantitative assessment of arterial wall biomechanical properties using shear wave imaging. Ultrasound Med Biol. 2010; 36:1662–1676. [PubMed: 20800942]

Derieppe M, Delmas Y, Gennisson JL, Deminière C, Placier S, Tanter M, Combe C, Grenier N. Detection of intrarenal microstructural changes with supersonic shear wave elastography in rats. Eur Radiol. 2012; 22:243–250. [PubMed: 21845464]

Dolenšek J, Rupnik MS, Stožer A. Structural similarities and differences between the human and the mouse pancreas. Islets. 2015; 7:e1024405. [PubMed: 26030186]

Fatemi M, Greenleaf JF. Ultrasound-Stimulated Vibro-Acoustic Spectrography. Science (80-). 1998; 280:82–85.

Gallotti A, D'Onofrio M, Pozzi Mucelli R. Acoustic Radiation Force Impulse (ARFI) technique in ultrasound with Virtual Touch tissue quantification of the upper abdomen. Radiol Med. 2010; 115:889–897. [PubMed: 20082227]

Gennisson JL, Grenier N, Combe C, Tanter M. Supersonic Shear Wave Elastography of In Vivo Pig Kidney: Influence of Blood Pressure, Urinary Pressure and Tissue Anisotropy. Ultrasound Med Biol. 2012; 38:1559–1567. [PubMed: 22698515]

Godfrey EM, Mannelli L, Griffin N, Lomas DJ. Magnetic resonance elastography in the diagnosis of hepatic fibrosis. Semin Ultrasound CT MR Elsevier. 2013; 34:81–88.

Guo J, Hirsch S, Streitberger KJ, Kamphues C, Asbach P, Braun J, Sack I. Patient-activated three-dimensional multifrequency magnetic resonance elastography for high-resolution mechanical imaging of the liver and spleen. RoFo Fortschritte auf dem Gebiet der Rontgenstrahlen und der Bildgeb Verfahren. 2014; 186:260–266.

Hingorani SR, Iii EFP, Maitra A, Rajapakse V, King C, Jacobetz MA, Ross S, Conrads TP, Veenstra TD, Hitt BA, Kawaguchi Y, Johann D, Liotta LA, Crawford HC, Putt ME, Jacks T, Wright CVE, Hruban RH, Lowy AM, Tuveson DA. Preinvasive and invasive ductal pancreatic cancer and its early detection in the mouse. Cancer Cell. 2003; 4:437–450. [PubMed: 14706336]

Hingorani SR, Wang L, Multani AS, Combs C, Deramaudt TB, Hruban RH, Rustgi AK, Chang S, Tuveson Da. Trp53R172H and KrasG12D cooperate to promote chromosomal instability and widely metastatic pancreatic ductal adenocarcinoma in mice. Cancer Cell. 2005; 7:469–483. [PubMed: 15894267]

Hou G, Provost J, Grondin J, Wang S, Marquet F, Bunting E, Konofagou E. Sparse matrix beamforming and image reconstruction for real-time 2D HIFU monitoring using Harmonic Motion Imaging for Focused Ultrasound (HMIFU) with in vitro validation. IEEE Trans Med Imaging. 2014

Hruban RH, Pitman MB, Klimstra DS. Tumors of the pancreas (Vol. 6). American Registry of Pathology. 2007

Kerdok AE, Ottensmeyer MP, Howe RD. Effects of perfusion on the viscoelastic characteristics of liver. J Biomech. 2006; 39:2221–2231. [PubMed: 16126215]

Konofagou EE, Hynynen K. Localized harmonic motion imaging: theory, simulations and experiments. Ultrasound Med Biol. 2003; 29:1405–1413. [PubMed: 14597337]

Kruse SA, Smith JA, Lawrence AJ, Dresner MA, Manduca A, Greenleaf JF, Ehman RL. Tissue characterization using magnetic resonance elastography : preliminary results. Phys Med Biol. 2000; 45:1579–1590. [PubMed: 10870712]

Leung VY, Shen J, Wong VW, Abrigo J, Wong GL, Chim AM, Chu SH, Chan AW, Choi PC, Ahuja AT, Chan HL, Chu WC. Quantitative elastography of liver fibrosis and spleen stiffness in chronic hepatitis B carriers: comparison of shear-wave elastography and transient elastography with liver biopsy correlation. Radiology. 2013; 269:910–918. [PubMed: 23912619]

Lowenfels AB, Maisonneuve P. Epidemiology and risk factors for pancreatic cancer. Best Pract Res Clin Gastroenterol. 2006; 20:197–209. [PubMed: 16549324]

Luo J, Konofagou E. A fast normalized cross-correlation calculation method for motion estimation. IEEE Trans Ultrason Ferroelectr Freq Control. 2010; 57:1347–1357. [PubMed: 20529710]

Maleke C, Pernot M, Konofagou EE. Single-Element Focused Ultrasound Transducer Method for Harmonic Motion Imaging. Ultrason Imaging. 2006; 28:144–158. [PubMed: 17147056]

Masuzaki R, Tateishi R, Yoshida H, Sato T, Ohki T, Goto T, Yoshida H, Sato S, Sugioka Y, Ikeda H, Shiina S, Kawabe T, Omata M. Assessing liver tumor stiffness by transient elastography. Hepatol Int. 2007; 1:394–397. [PubMed: 19669335]

Mauldin FW, Haider MA, Loboa EG, Behler RH, Euliss LE, Pfeiler TW, Gallippi CM. Monitored steady-state excitation and recovery (MSSER) radiation force imaging using viscoelastic models. IEEE Trans Ultrason Ferroelectr Freq Control. 2008; 55:1597–1610. [PubMed: 18986950]

Muthupillai R, Lomas DJ, Rossman PJ, Greenleaf JF, Manduca A, Ehman RL. Magnetic resonance elastography by direct visualization of propagating acoustic strain waves. Science (80-). 1995; 269:1854–1857.

Nightingale KR, Palmeri ML, Nightingale RW, Trahey GE. On the feasibility of remote palpation using acoustic radiation force. J Acoust Soc Am. 2001; 110:625. [PubMed: 11508987]

Olive KP, Jacobetz MA, Davidson CJ, Gopinathan A, McIntyre D, Honess D, Madhu B, Goldgraben MA, Caldwell ME, Allard D, Frese KK, Denicola G, Feig C, Combs C, Winter SP, Ireland-Zecchini H, Reichelt S, Howat WJ, Chang A, Dhara M, Wang L, Rückert F, Grützmann R, Pilarsky C, Izeradjene K, Hingorani SR, Huang P, Davies SE, Plunkett W, Egorin M, Hruban RH, Whitebread N, McGovern K, Adams J, Iacobuzio-Donahue C, Griffiths J, Tuveson DA. Inhibition of Hedgehog signaling enhances delivery of chemotherapy in a mouse model of pancreatic cancer. Science (80-). 2009; 324:1457–1461.

Ophir J, Alam S, Garra B. Elastography: imaging the elastic properties of soft tissues with ultrasound. J Med Ultrason. 2002; 29:155–171.

Palmeri ML, Wang MH, Dahl JJ, Frinkley KD, Nightingale KR. Quantifying hepatic shear modulus in vivo using acoustic radiation force. Ultrasound Med Biol. 2008; 34:546–558. [PubMed: 18222031]

Parker KJ, Huang SR, Musulin Ra, Lerner RM, Musulin. Tissue Response to Mechanical Vibrations for “Sonoelastic Imaging”. Ultrasound Med Biol. 1990; 16:241–246. [PubMed: 2194336]

Ries M, De Senneville BD, Roujol S, Berber Y, Quesson B, Moonen C. Real-time 3D target tracking in MRI guided focused ultrasound ablations in moving tissues. Magn Reson Med. 2010; 64:1704–1712. [PubMed: 20878763]

Salameh N, Abarca-quinones J, Leclercq I, Fink M, Sinkus R, Beers BE Van. Early Detection of Steatohepatitis in Fatty Rat Liver by using MR Elastography. Radiology. 2009; 253

Sandrin L, Fourquet B, Hasquenoph J-M, Yon S, Fournier C, Mal F, Christidis C, Ziol M, Poulet B, Kazemi F, Beaugrand M, Palau R. Transient elastography: a new noninvasive method for assessment of hepatic fibrosis. Ultrasound Med Biol. 2003; 29:1705–1713. [PubMed: 14698338]

Sapin-de Brosses E, Pernot M, Tanter M. The link between tissue elasticity and thermal dose in vivo. Phys Med Biol. 2011; 56:7755–7765. [PubMed: 22094357]

Sarvazyan A, Rudenko O, Swanson S, Fowlkes J, Emelianov SY. Shear wave elasticity imaging: a new ultrasonic technology of medical diagnostics. Ultrasound Med Biol. 1998; 24:1419–1435. [PubMed: 10385964]

Sastra SA, Olive KP. Pancreatic Cancer. Pancreat Cancer Methods Protoc. 2013:249–266.

Shah NS, Kruse SA, Lager DJ, Farell-Baril G, Lieske JC, King BF, Ehman RL. Evaluation of renal parenchymal disease in a rat model with magnetic resonance elastography. Magn Reson Med. 2004; 52:56–64. [PubMed: 15236367]

Shi X, Martin RW, Rouseff D, Vaezy S, Crum La. Detection of high-intensity focused ultrasound liver lesions using dynamic elastometry. Ultrason Imaging. 1999; 21:107–126. [PubMed: 10485565]

Siegel R, Ma J, Zou Z, Jemal A. Cancer Statistics. 2014; 64:9–29. 2014.

Steiniger BS. Human spleen microanatomy: why mice do not suffice. Immunology. 2015; 145:334–346. [PubMed: 25827019]

Umale S, Deck C, Bourdet N, Dhumane P, Soler L, Marescaux J, Willinger R. Experimental mechanical characterization of abdominal organs: Liver, kidney & spleen. J Mech Behav Biomed Mater Elsevier. 2012; 17:22–33.

Vappou J, Hou GY, Marquet F, Shahmirzadi D, Grondin J, Konofagou EE. Non-contact, ultrasound-based indentation method for measuring elastic properties of biological tissues using Harmonic Motion Imaging (HMI). Phys Med Biol IOP Publishing. 2015; 60:2853–2868.

Vappou J, Maleke C, Konofagou EE. Quantitative viscoelastic parameters measured by harmonic motion imaging. Phys Med Biol. 2009; 54:3579–3594. [PubMed: 19454785]

Vizzutti F, Arena U, Romanelli RG, Rega L, Foschi M, Colagrande S, Petrarca A, Moscarella S, Belli G, Zignego AL, Marra F, Laffi G, Pinzani M. Liver stiffness measurement predicts severe portal hypertension in patients with HCV-related cirrhosis. Hepatology. 2007; 45:1290–1297. [PubMed: 17464971]

Wang J, Guo L, Shi X, Pan W, Bai Y, Ai H. Real-time elastography with a novel quantitative technology for assessment of liver fibrosis in chronic hepatitis B. Eur J Radiol Elsevier Ireland Ltd. 2012; 81:e31–e36.

Wang MH, Palmeri ML, Guy CD, Yang L, Hedlund LW, Diehl AM, Nightingale KR. In vivo quantification of liver stiffness in a rat model of hepatic fibrosis with acoustic radiation force. Ultrasound Med Biol. 2009; 35:1709–1721. [PubMed: 19683381]

Yin M, Talwalkar JA, Glaser KJ, Manduca A, Grimm RC, Rossman PJ, Fidler JL, Ehman RL. Assessment of hepatic fibrosis with magnetic resonance elastography. Clin Gastroenterol Hepatol. 2007a; 5:1207.e2–1213.e2. [PubMed: 17916548]

Yin M, Woollard J, Wang X, Torres VE, Harris PC, Ward CJ, Glaser KJ, Manduca A, Ehman RL. Quantitative assessment of hepatic fibrosis in an animal model with magnetic resonance elastography. Magn Reson Med. 2007b; 58:346–353. [PubMed: 17654577]

Zachiu C, Denis de Senneville B, Moonen C, Ries M. A framework for the correction of slow physiological drifts during MR-guided HIFU therapies: Proof of concept. Med Phys. 2015; 42:4137–4148. [PubMed: 26133614]

Zhu Y, Zhang X, Zheng Y, Chen X, Shen Y, Lin H, Guo Y, Wang T, Chen S. Quantitative analysis of liver fibrosis in rats with shear wave dispersion ultrasound vibrometry: Comparison with dynamic mechanical analysis. Med Eng Phys Institute of Physics and Engineering in Medicine. 2014; 36:1401–1407.

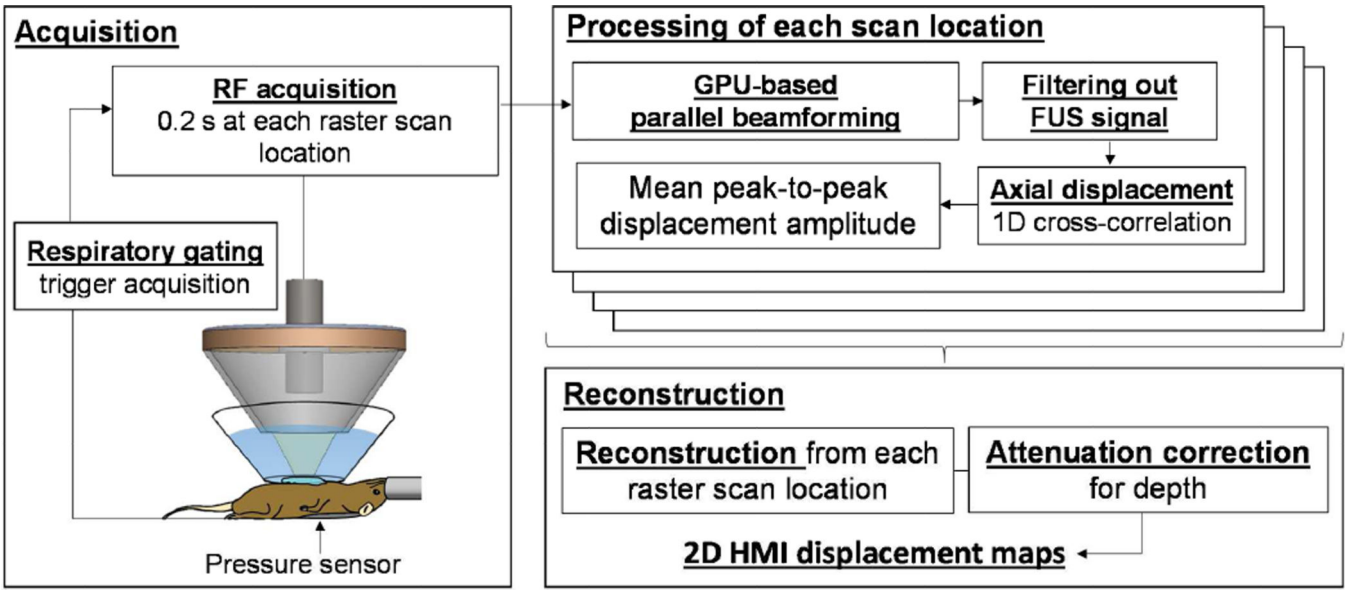

Figure 1.

Illustration of the experimental setup and the processing performed to obtain HMI displacement maps *in vivo*.

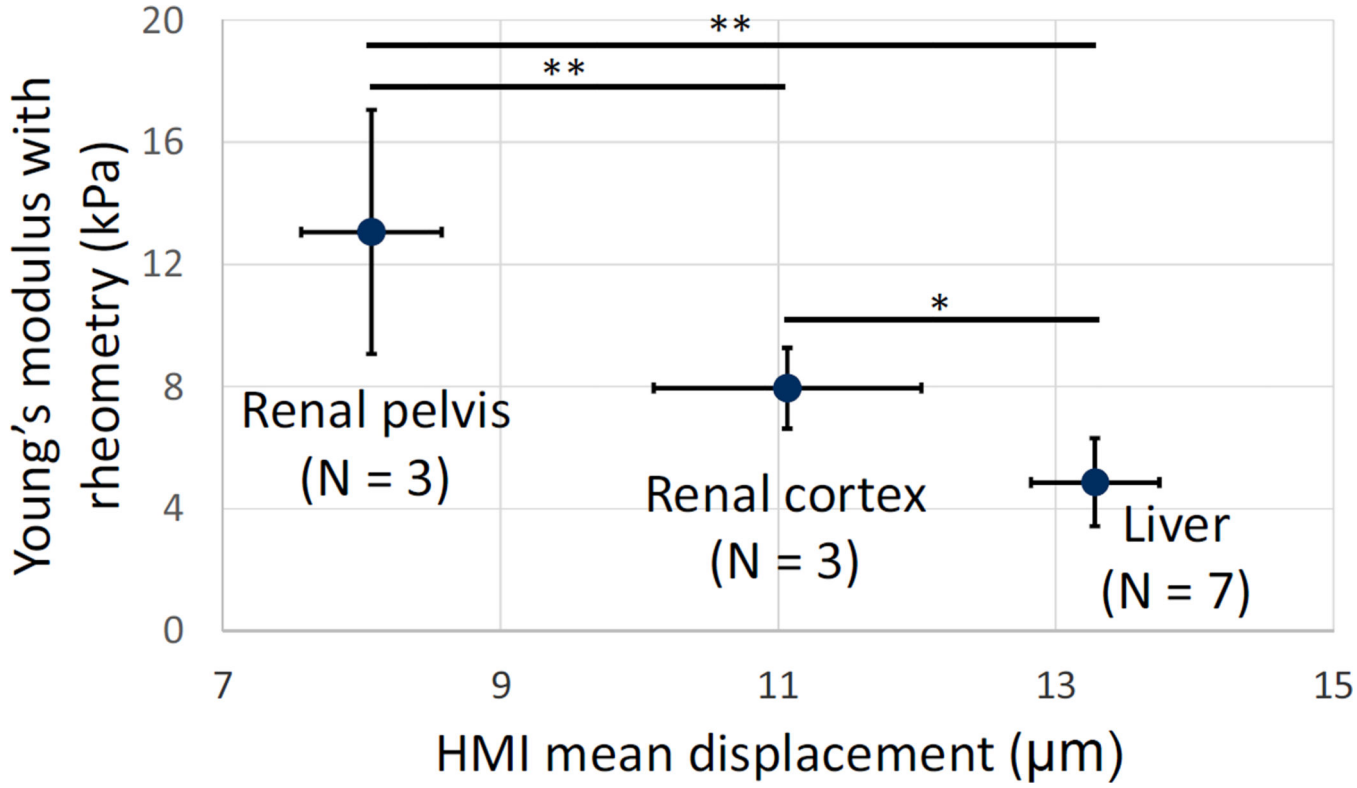

Figure 2.

Comparison of Young's moduli obtained with rheometry against HMI displacement in *in vitro* canine liver, renal cortex and renal pelvis (Two-tail T-test: * $p < 0.05$, ** $p < 0.01$).

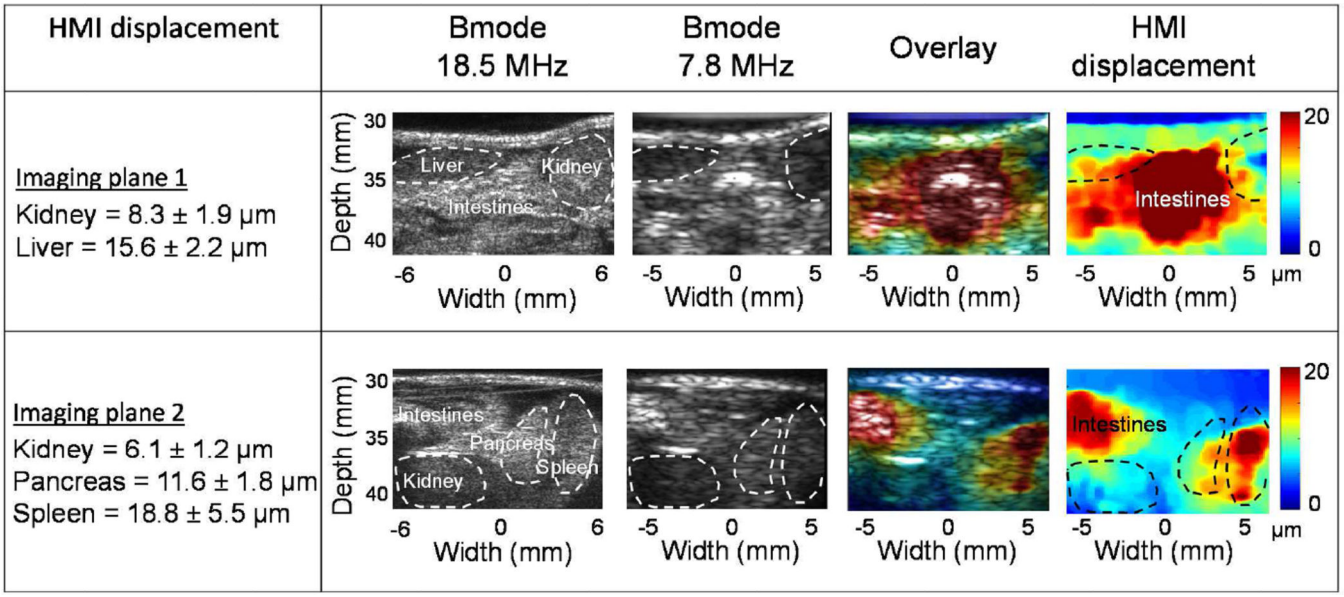

Figure 3.

Bmode images and HMI elasticity maps obtained *in vivo* in two planes from the same mouse. Imaging plane #1 (first row) shows the kidney and the liver separated by intestines. The second plane displays the pancreas, the spleen and the kidney.

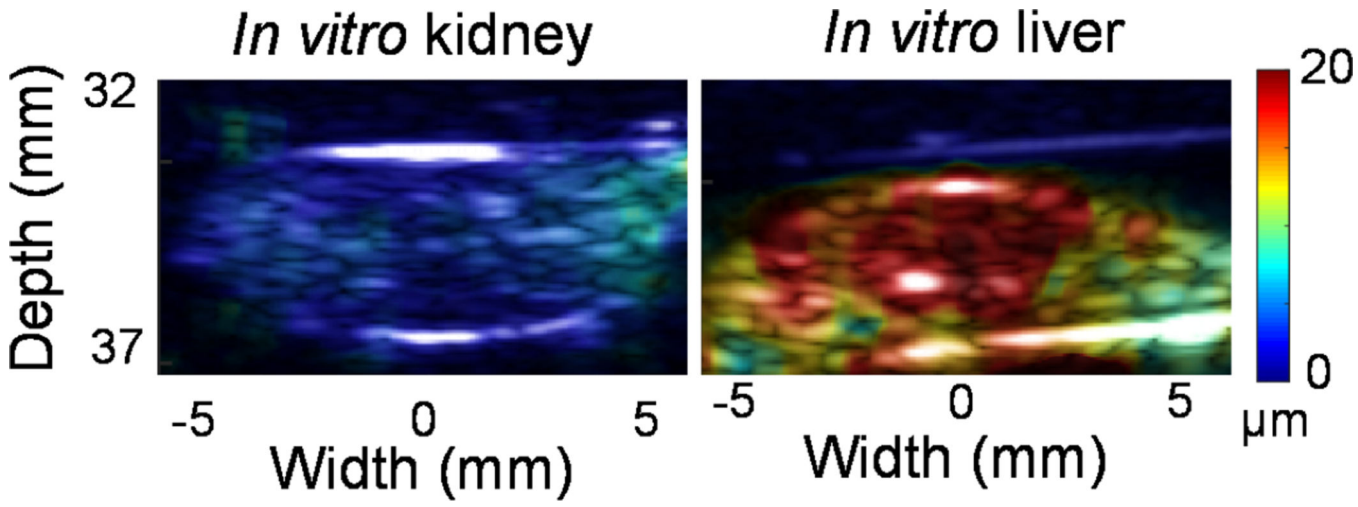

Figure 4.
HMI displacement maps overlaid on Bmode images obtained *ex vivo* in the kidney and the liver of the mouse shown in Figure 3.

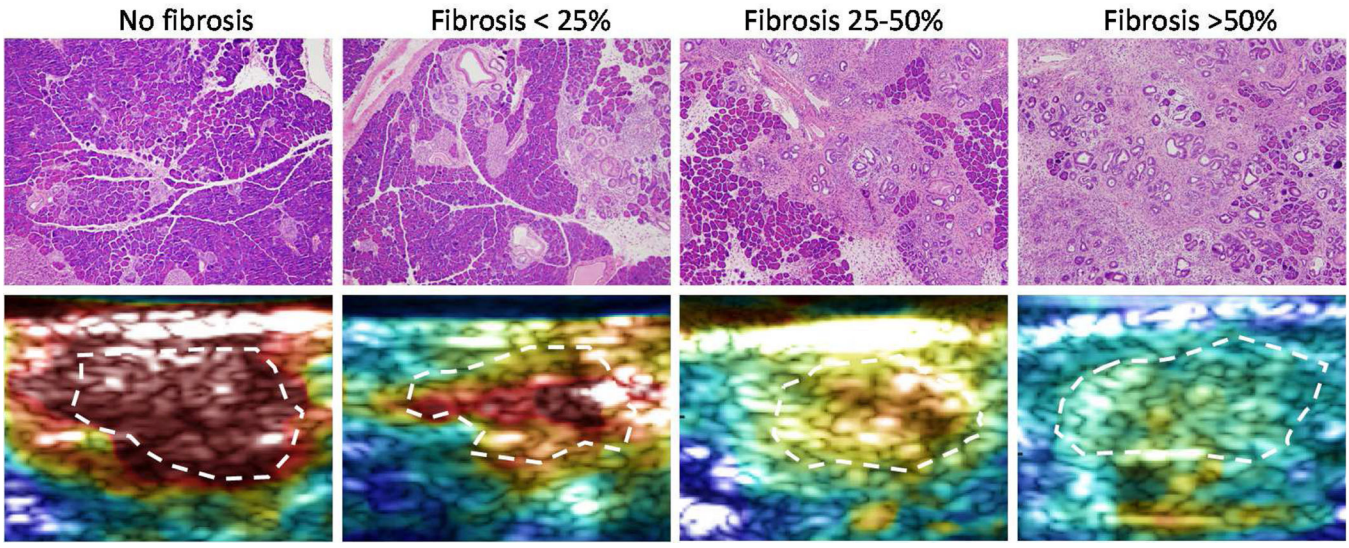

Figure 5.

H&E stained slides of pancreas with different degrees of fibrosis (10× magnification). The corresponding HMI displacement maps overlaid on Bmode images are also shown below.

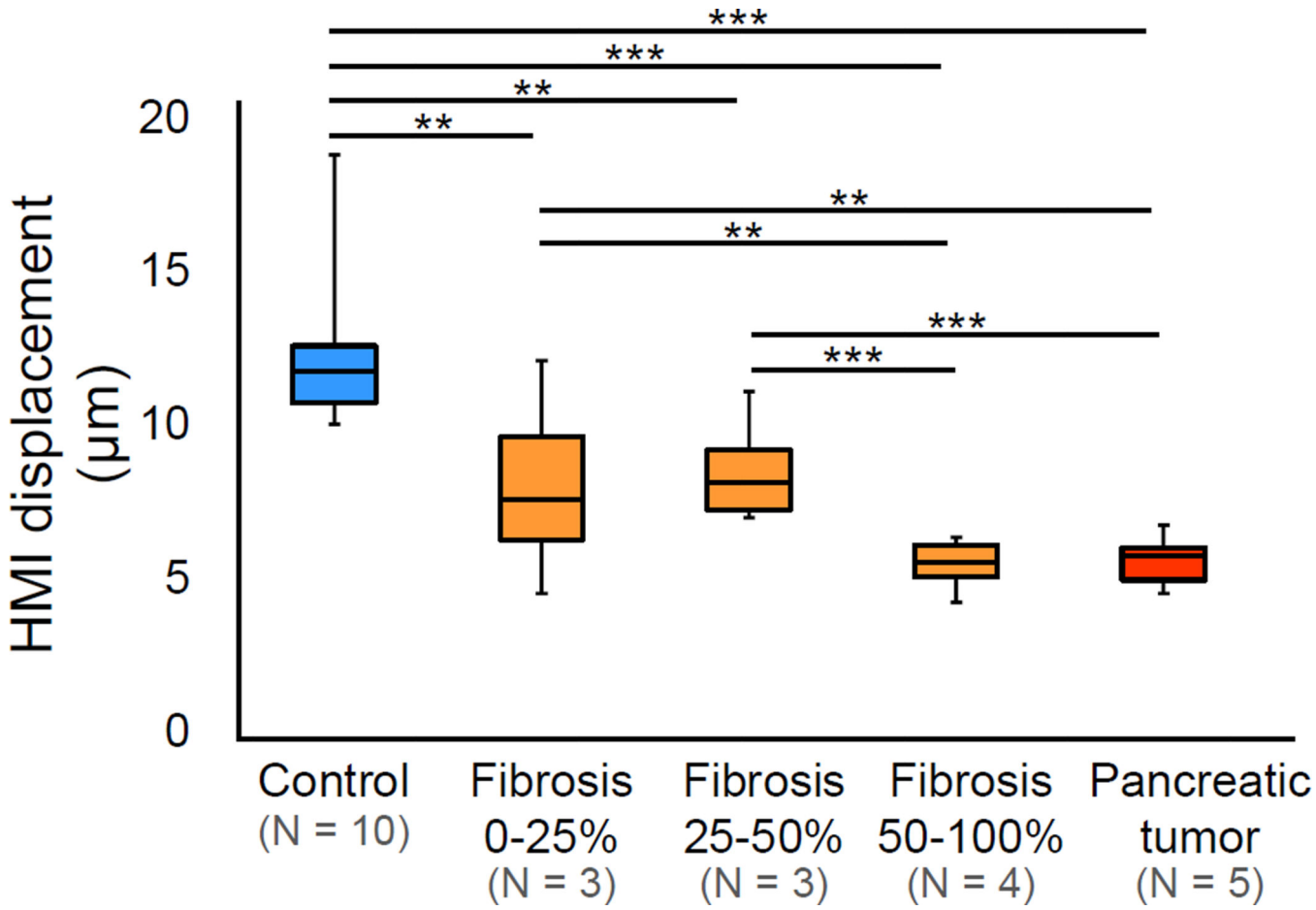

Figure 6.

HMI displacements measured *in vivo* in normal pancreas, in inflamed pancreas with different stages of fibrosis, and in pancreatic tumors (Two-tail T-test: ** p <0.01, *** p < 0.001).

Table 1

HMI displacements measured *in vivo* in murine spleen, liver, pancreas, and kidney (N = 10).

Organs	Spleen	Liver	Pancreas	Kidney
Displacement (μm)	18.3 ± 7.0	14.2 ± 2.1	12.3 ± 2.5	6.3 ± 1.9